Biointerface Research in Applied Chemistry
Open-Access Journal (ISSN: 2069-5837)

Article
Volume 16, Issue 4, 2026, 120
https://doi.org/10.33263/BRIAC164.120

Facile Synthesis and Electromagnetic Interference Shielding Performance of Pani-Decorated Tetraamino Metal Phthalocyanine Nanocomposites and their Electrochemical Sensing of L-Cysteine

Nydile Thirthahalli Nagaraj [1], Jadiyappa Sannappa [1,*], Malathesh Pari [2]

[1] Department of PG Studies and Research in Physics, Kuvempu University, Shankaraghatta-577451, Karnataka, India; nydiletn@gmail.com (N.T.N); sannappaj2012@gmail.com (J.S);
[2] Department of Chemistry, BGS Institute of Technology (BGSIT), Adichunchanagiri University, B G Nagar, Nagamangala, Mandya-571448, Karnataka, India; malateshpari@BGSIT.ac.in (M.P);
* Correspondence: sannappaj2012@gmail.com;

Received: 6.04.2023; Accepted: 28.05.2023; Published: 15.08.2026

Abstract: This paper describes the synthesis of tetraamino metal phthalocyanine (TAMPc) ingrained polyaniline (PANI) and their characterization by spectroscopic techniques. Additionally, this work presents the electromagnetic interference (EMI) shielding performance of polyaniline doped tetra amino metal phthalocyanine (PANI-TAMPc) and the electrochemical detection of L-Cysteine. The spectroscopic characterization of the synthesized PANI-TAMPcs was performed using XRD, FTIR, SEM, TGA, and UV-Vis techniques. The variation in the dielectric constant and conductivity of PANI-TAMPc nanocomposites with frequency was undertaken in the frequency range 40 Hz-5 MHz using an impedance analyzer. Additionally, the Electromagnetic Interference Shielding performance of hybrid PANI-TAMPcs was studied using a Vector Network Analyzer. PANI-TACo(II)Pc is highly efficient among PANI-TAMPc nanocomposites, with an adequate total EMI shielding effectiveness (SET) of 40dB in the X-band, due to the increase in surface area and heterogeneous phase components in their moieties. Also, the PANI-TACo(II)Pc/GC electrode exhibits good sensing performance for L-cysteine and shows a very good analytical profile, including a long linear range, sensitivity, and detection limit of 0.5-3.5 µM, 0.1198 µA/µM, and 0.166 µM, respectively. Also, this sensor shows repeatability and stability without any leaching property. Therefore, our study suggests that PANI-TACo(II)Pc can be a good choice as an excellent EMI shielding material for EMI applications and for sensing L-cysteine.

Keywords: phthalocyanine; L-cysteine; AC conductivity; EMI shielding; cyclic voltammetry.

1. Introduction

The extensive use of electronic devices and the rapid development in science & technology can induce electromagnetic interference (EMI) [1]. EMI is mainly created by electromagnetic noise. Radiation emitters, such as mobile phones, laptops, computers, telecommunication equipment, and power cables, present in the environment, will generate electromagnetic noise. The performance of electronic devices/electrical circuits degrades due to Electromagnetic radiation, which also affects biological activities, including human and animal health [2]. To reduce electromagnetic signal interference, it is essential to develop EMI

shielding materials that effectively attenuate electromagnetic waves through reflection and absorption [3].

For the interaction with the electromagnetic field in radiation, the shielding material should bear mobile charge carriers [4]. Generally, electrically conductive polymer nanocomposites are preferred due to their attractive properties: flexibility, light weight, corrosion resistance, electrical conductivity, and lower density. Polyaniline has drawn significant interest due to its attractive properties, including processability, stability, and electrical conductivity, among other electrically conductive polymers [5]. The nanocomposites of conductive polyaniline and metal complexes exhibit a variety of applications, such as low density, increased hardness, and enhanced electromagnetic properties, and they have also drawn much attention because of their novel dielectric, magnetic, and electrically conducting properties [6].

Phthalocyanines (Pcs) are a class of metal–organic complexes characterized by their blue-green coloration and semiconducting behavior. They belong to the family of aromatic, heterocyclic, π-conjugated compounds, featuring an extended molecular structure with alternating single and double bonds [7]. Phthalocyanine derivatives possess an extended delocalized π-electron system [8], while the degree of π-electron delocalization and its interaction with the central metal ion in tetra-amino metal phthalocyanines (TAMPcs) play a significant role in governing their redox behavior [9]. Their chemical and thermal stabilities are essential properties that make them suitable for incorporation into electrochemical sensors [10-13]. The polymeric Pcs possess a conjugated structure and are stable against light, heat, and moisture. Hence, polymeric phthalocyanines can be better used as environmentally stable, electrically conductive, and EMI shielding material. Polymeric tetraamino-metallo-phthalocyanines of Cobalt (Co), Nickel (Ni), and Iron (Fe) acquire a large, wide conjugated structure and exhibit high electrical conductivity. Among them, PANI-TACo(II)Pc exhibits greater conductivity and EMI shielding effectiveness than PANI-TAFe(II)Pc, PANI-TANi(II)Pc, and PANI-TACu(II)Pc [14,15].

The most essential amino acid is L-cysteine (L-Cys). It plays a prominent role in biological systems and has been widely used in the food and medical industries. Moreover, in a variety of biological media, L-cysteine is usually used as a model for the role of the thiol group and disulfide bond in proteins [16]. Therefore, determining L-Cys is very important. In physicochemical analysis, the rapid detection of nanomolar and micro quantities of ionic species using the simplest methods is of great significance. The TACo(II)Pc–PANI-modified glassy carbon electrode offers a simple and efficient platform for the electrochemical detection of L-cysteine, providing advantages such as facile electrode fabrication, rapid analysis, minimal handling requirements, and ease of operation [17]. Finally, our work indicates that the EMI shielding effectiveness of the polyaniline matrix is enhanced by the incorporation of tetra-aminocobalt(II) phthalocyanines, paving the way for the fabrication of simple, lightweight, and environmentally friendly microwave attenuation materials for better EMI applications.

2. Materials and Methods

2.1. Materials.

Aniline (99% purity), 4-nitrophthalic anhydride, NH_4Cl, HCl, sodium sulfide nanohydrate, and ammonium persulfate (APS) were purchased from Sigma-Aldrich. TAMPc was prepared using a well-

established literature method [18]. DMF was purchased from Sigma-Aldrich. All other Reagents were purchased from Merck, and we used double-distilled water in this work.2.1.1. Methods.

EMI shielding measurements were undertaken using a Vector Network Analyzer at MSRIT Bangalore, and AC conductivity was measured using an Impedance analyzer. IR Spectra were reported using a Shimadzu spectrometer; UV-Visible Spectra were carried out using a Shimadzu 1800; TGA of the sample was performed using an SDT Q600 in an N2 atmosphere at USIC, Karnatak University, Dharwad (KUD). SEM analysis of the sample was obtained using a JSM-IT500 at SAIF in KUD. XRD analysis was performed using a crystal XRD at PURSE, Mangalore University. The CVs were carried out using a CHI1608D electrochemical workstation (USA) at SSC Shimoga.

2.1.2. Synthesis of tetra nitro metal phthalocyanine(TNMPc).

The TNMPc was synthesized by grounding the blend of NH_4Cl (1.46g,0.03mol), urea, 4-nitro phthalic anhydride (9.96g, 0.05mol), $(NH_4)_6Mo_7O_{24}$ (0.5g, 0.4mmol), and required metal salts (0.06 mol) [Fe, Co, Ni chlorides]. This finely blended mixture was poured into an RB flask containing $C_6H_5NO_2$ (50ml). The mixture was stirred at 120-190 ℃ using a mechanical Stirrer for 5 hours. A greenish Solid was obtained and filtered through Whatman filter paper. The sample was initially washed with methanol, then with hot deionized water, and finally with a hot dilution of HCl and methanol until a colorless filtrate was obtained. The pure TNMPc was dried for 12 hours at 80 ℃, yielding a greenish TNMPc powder [18].

2.1.3. Synthesis of tetra amino metal phthlocyanine(TAMPc):[M= Co, Fe and Ni].

TAFePc was prepared in accordance with the literature procedure [19]. To modify the procedure of the above-titled compound. The compound TNFePc (2 g, 2.6 mM) was transferred into an RB flask containing 30 mL DMF, and the sodium sulfide nanohydrate (7.5g, 40.0 millimoles) precursor was added to the reaction mixture.

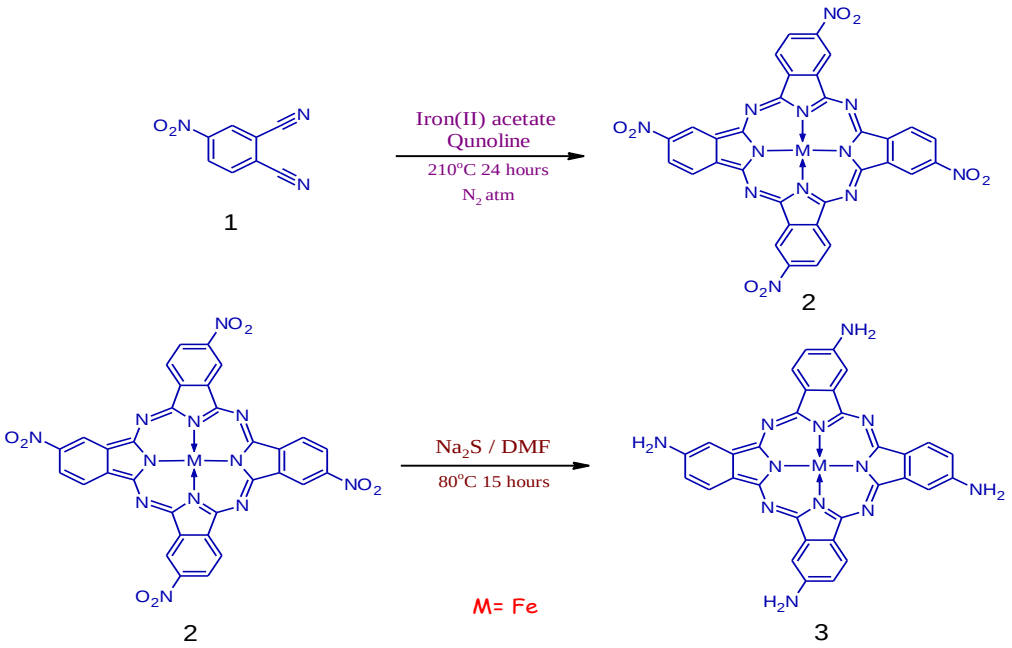

Scheme 1. Synthesis of Tetra Amino metal Phthalocyanine[M= Co, Fe, and Ni].

Further, the blended mixture was stirred at a temperature of 80 ℃ under aqueous conditions for 4 hours. After 4 hours, the reaction mixture was allowed to cool to room

temperature, then poured into cold water. Upon centrifugation, the PPT was collected, and the resulting compound was washed with methanol, then with hot water. The pure compound was dried in a hot air oven. The synthesized TAFe(II)Pc was obtained in blue/green color. Similarly, the same procedure was followed in the synthesis of Co(II)Pc and Ni(II)Pc as shown in Scheme 1.

2.1.4. Synthesis of polyaniline(PANI).

The synthesis of PANI was done by oxidative polymerization reaction using APS[$(NH_4)_2S_2O_8$]. 4.56 g of fresh aniline was taken in a 100 mL beaker consisting of 25 mL of 1N HCl, and 5.704 g of APS was added rapidly to the reaction mixture. The reaction mixture was kept at 5 ℃ under constant stirring in a magnetic stirrer for 4-6 hours. A thick green precipitate was obtained and filtered. The obtained crude compound was washed with dilute HCl until a colorless filtrate was obtained. The pure PANI compound was dried in an oven at 60 ℃ for 12 hours to get the synthesized sample [20].

2.1.5. Preparation of polyaniline decorated TAMPc nanocomposite.

TAFe(II) Pc-impregnated PANI nanocomposite was synthesized at room temperature using a stepwise sonication method. 0.2g of aniline was taken in a 100 mL beaker containing 12 mL of 1N HCl. For that, 0.25 g of TAFe(II)Pc was added. It was sonicated for an hour at room temperature. Afterward, 0.4 g of APS was added to the reaction mixture and stirred for 5 minutes using a magnetic stirrer. The reaction mixture was kept undisturbed for 8 hours to promote polymerization. Later, the reaction mixture was filtered and washed with methanol, then with deionized water. The pure compound obtained was dried in a hot air oven at 80 ℃ to get dark greenish coloured TAFe(II)Pc-PANI nano composite. Similarly, the same procedure was used to prepare TACo(II)Pc-PANI and TANi(II)Pc-PANI nano-composites [21].

3. Results and Discussion

3.1. Electronic spectra.

The UV-Visible spectra of synthesized PANI, TACo(II)Pc, and PANI-TAMPc nanocomposite were obtained using DMF as the solvent and are shown in Figure 1. The UV-Vis absorption spectrum of polyaniline showed that the B-band was found in the Ultraviolet region at 300nm and the Q-band in the visible region at 630nm. Compared to the absorption spectra of PANI and TACo(II)Pc, the B-band was found in the UV region at 310nm and the Q-band in the visible region at 645nm. Meanwhile, the absorption spectra of TAFePc-PANI nanocomposite showed the B-band at 340nm and the Q-band at 732nm. Similarly, TACo(II)Pc-PANI and TANiPc-PANI showed a B-band at 340nm and 347nm, respectively, and a Q-band at 731nm and 630nm, respectively. The PANI-TAMPc also showed a shoulder peak at 664 nm for TAFe(II)Pc-PANI, at 662 nm for TACo(II)Pc-PANI, and at 630 nm for TANi(II)Pc-PANI. Aggregation in the TAMPc-PANI complex is indicated by a broadened or split Q-band, with the high-energy band arising from the aggregate and the low-energy band from the monomer. The Q-band of the PANI-TAFe(II)Pc spectrum exhibits one very broad aggregated peak at 732nm. This affirms the monomeric nature of the PANI-TAFe(II)Pc. The spectroscopic data confirm the embedding of the three species, such as PANI, TACo(II)Pc, and PANI-TAMPcs [21,22].

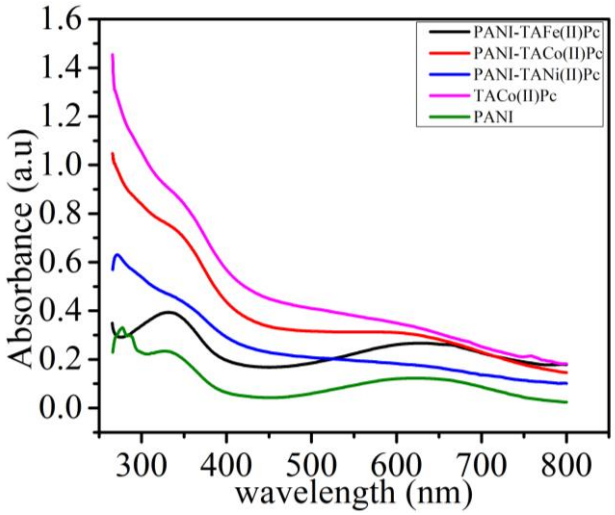

Figure 1. UV-visible spectrum of PANI-TAMPcs, TACo(II)Pc, and PANI.

3.2. Infrared spectral studies.

FT-IR spectroscopy confirms the formation of the PANI-TAMPc nanocomposite, as shown in Figure 2. The FT-IR spectrum of PANI nanofibre exhibits peaks at 1587 cm^{-1} and 1423cm^{-1} for C-N and C=C stretching of quinonoid and benzenoid rings of PANI nanofibres, and TACo(II)Pc indicates a peak at 1676 cm^{-1} and 1599 $cm^{-1}$for the NH deformation and C=N stretching of phthalocyanine, respectively[10]. The N-H peak for TACo(II)Pc appears at 3250cm^{-1}. In the case of PANI-TAMPc, the NH peak has been shifted to a lower wavenumber region. Hence, this confirms the existence of some interaction between PANI and TAMPc and also the formation of a polymer nanocomposite. While the TACo(II)Pc dopedPANI nanofibre shows peaks at 1594 cm^{-1} and 1427 cm^{-1}, TANi(II)Pc doped PANI nanofibre shows peak at 1597 cm^{-1} and 1422 cm^{-1}, TAFe(II)Pc doped PANI nanofibre shows peak at 1592 cm^{-1} and 1428 cm^{-1} respectively are the characteristic peak of PANI nanofibres and the remaining peaks at 1308 cm^{-1}, 1148 cm^{-1}, 1084 cm^{-1}, 830 cm^{-1}, 753 cm^{-1} corresponds to the distinctive peaks of TAMPc which validates the TAMPc doped PANI nanofibre [22].

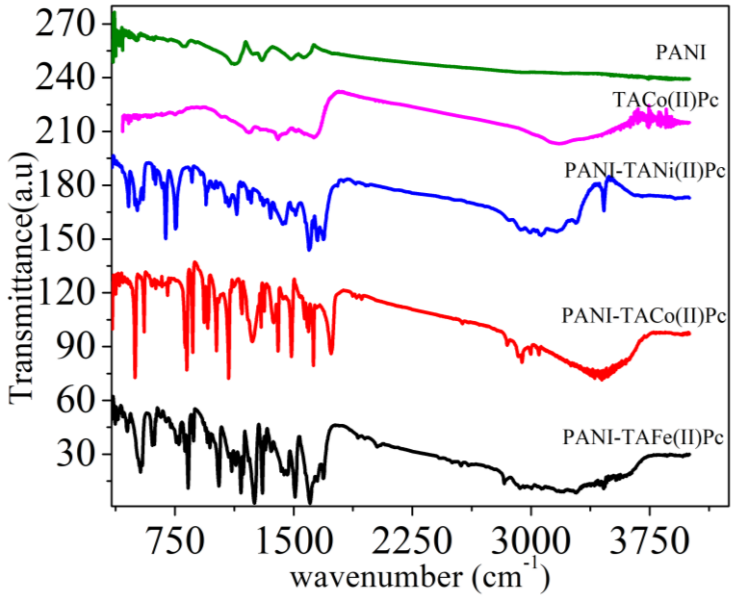

Figure 2. FT-IR Spectrum of PANI-TAMPcs, TACo(II)Pc, and PANI.

3.3. Thermogravimetric studies.

Figure 3 shows the thermogravimetric curves of the basic PANI, TACo(II)Pc, and PANI-TAMPc nanocomposites. According to TGA, the first-step degradation takes place in the range 50-120 ℃, and there is a weight loss for PANI, TACo(II)Pc, and the PANI-TAMPc nanocomposite, attributed to the ejection of water molecules from the nanocomposite structure. In the second stage, the weight loss of PANI, TACo(II)Pc, and PANI-TAMPc occurred at 450 ℃, 480 ℃, and 520 ℃, respectively, due to the loss of the dopant (HCl) and low-molecular-weight remnants. In the third stage, the TG curve of PANI shows a decline at 580 ℃; the TACo(II)Pc complex is distorted as the pyrolysis initiates and decomposes at 560 ℃. Similarly, the PANI-TAMPc nanocomposite decomposition takes place up to 600-640 ℃. After the decomposition of complexes up to 900 ℃, the horizontal curve can be observed due to the formation of metal oxides (Co-O). It is predicted that the PANI-TAMPc is more thermally stable than PANI and TACo(II)Pc [23].

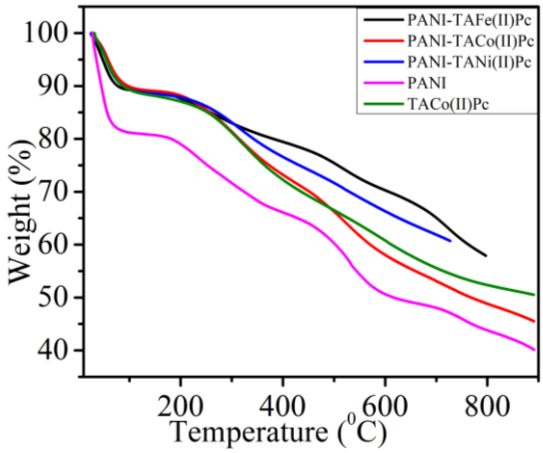

Figure 3. TGA of PANI-TAMPcs, TACo(II)Pc, and PANI.

3.4. SEM analysis.

Scanning electron microscopy has been employed to study the surface morphology of PANI and the PANI-TAMPc nanocomposite.

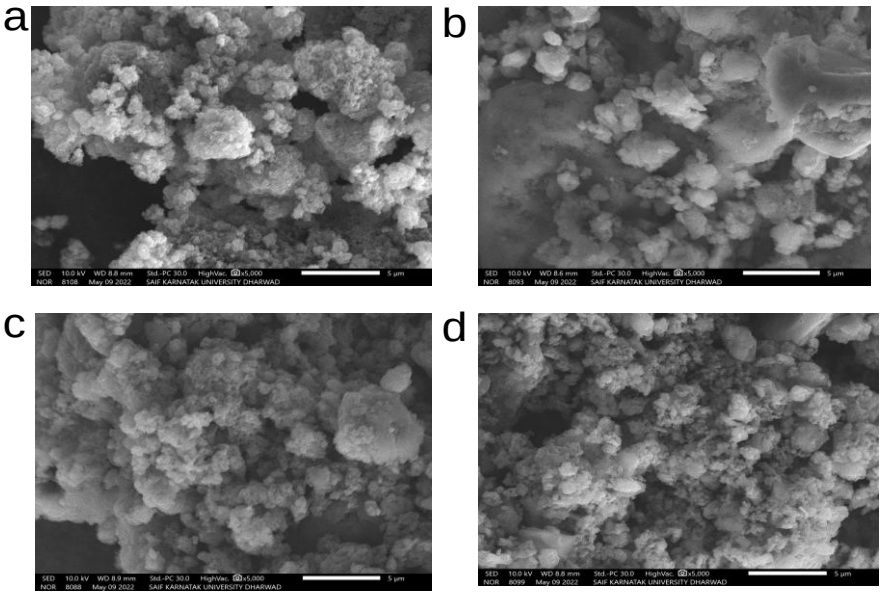

Figure 4. SEM images of **(a)**PANI;**(b)**PANI-TAFe(II)Pc;**(c)**PANI-TACo(II)Pc;**(d)** PANI-TANi(II)Pc.

The SEM image of polyaniline Figure 4 (a) represents an aggregated globular grainy structure with non-uniform morphology. The globular morphology is a very significant form for PANI prepared in an acidic aqueous medium [23]. The SEM studies performed for the PANI-TAMPc composite Figure 4 (b,c,d) reveal the presence of TAMPc particles covered by a polyaniline chain. This explains the successful composite formation and is mainly composed of irregularly arranged heterogeneous granular, non-porous, aggregated surface morphologies with diverse sizes. Such a morphology is very important for the material's excellent electromagnetic absorption properties.

3.5. XRD studies.

The crystalline nature of the amalgamated molecule was investigated using X-ray diffraction, as shown in Figure 5. In the XRD pattern of TACo(II)Pc, due to the lower crystallinity of the Pc macrocycle, a single broad peak can be observed in the region 2θ=26.35° [22,23]. In the XRD pattern of PANI-TACo(II)Pc, a small peak can be seen for PANI at 2θ=22.05°, which could be attributed to the crystal plane of polyaniline, and a broad peak was noted in the range of 2θ=24°-28° for the crystal plane of PANI and also TACo(II)Pc, which confirms the composite of PANI-TACo(II)Pc. Furthermore, it confirms the presence of the PANI-TAFe(II)Pc and PANI-TANi(II)Pc composites. The XRD analysis indicates that the synthesized sample is semicrystalline.

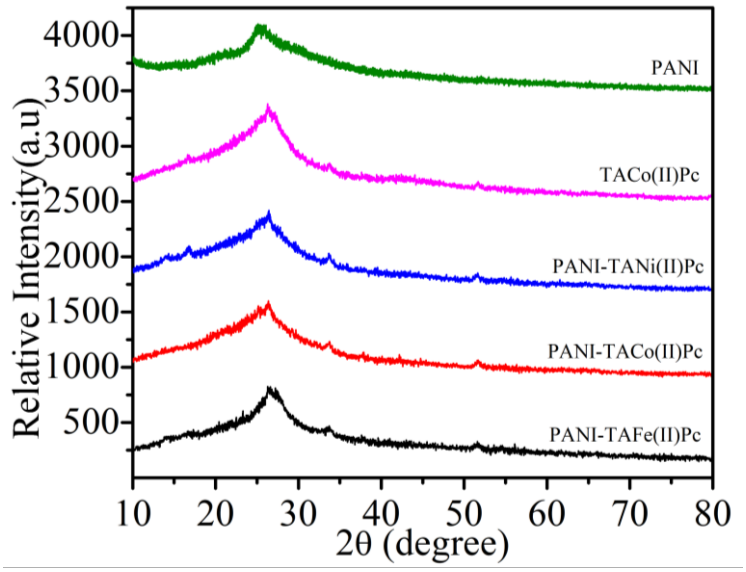

Figure 5. XRD images of PANI-TAMPcs, TACo(II)Pc, and PANI.

3.6. Dielectric studies.

The dielectric studies of PANI-TAMPc nanocomposites can be calculated using the relation [24].

$$C = \frac{\in_0 \varepsilon'}{d} A(1)$$

Where C is the capacitance of the synthesized sample, A is the surface area of the sample, $\in_0$ is the permittivity of air, and ϵ' is the dielectric permittivity of the sample. The variation of dielectric permittivity (ϵ') with frequency is shown in Figure 6. The dielectric permittivity of the sample decreases progressively as the applied frequency increases. This behavior can be attributed to the highly conjugated nature and extended planar molecular structure of TAMPc incorporated into the polyaniline matrix. There is a complete

delocalization of π electrons over the entire molecule. If the applied field increases, the probability of tunneling of electrons between the molecules also increases, causing a high dielectric loss and dielectric permittivity($\epsilon^{'}$). The observed variation in dielectric permittivity with frequency can be attributed to interfacial polarization arising from the Maxwell–Wagner mechanism, consistent with the principles proposed by Koop's phenomenological theory [25].

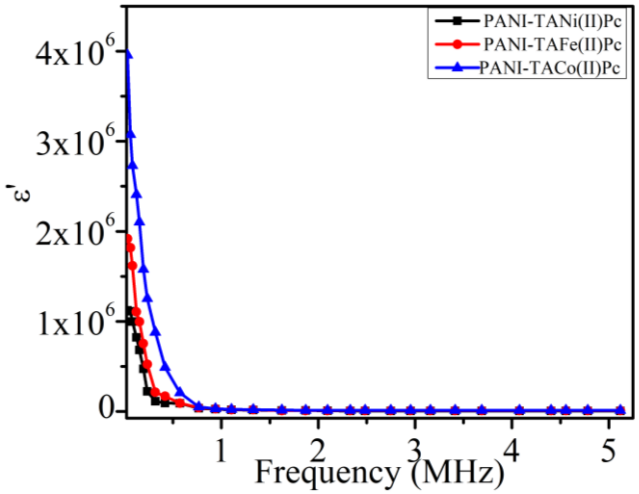

Figure 6. Frequency dependence of dielectric permittivity of PANI-TAMPcs.

At lower frequencies, the effect of grain boundaries is more predominant. The synthesized sample exhibits a high dielectric permittivity, which is ascribed to dislocations at grain boundaries, divalent positive ions, interfacial dislocations, and voids. At elevated frequencies, the dielectric permittivity becomes nearly frequency-independent, which can be attributed to the limited contribution of space-charge polarization associated with the heterogeneous distribution of highly conductive grains and comparatively resistive grain boundaries. As the frequency increases, the charge carriers have insufficient time to accumulate and follow the rapidly alternating electric field, thereby reducing the polarization response and resulting in lower dielectric permittivity values. Figure 6 indicates that PANI-TACo(II)Pc has a higher value of $\epsilon^{'}$ than PANI-TAFe(II)Pc and PANI-TANi(II)Pc [26].

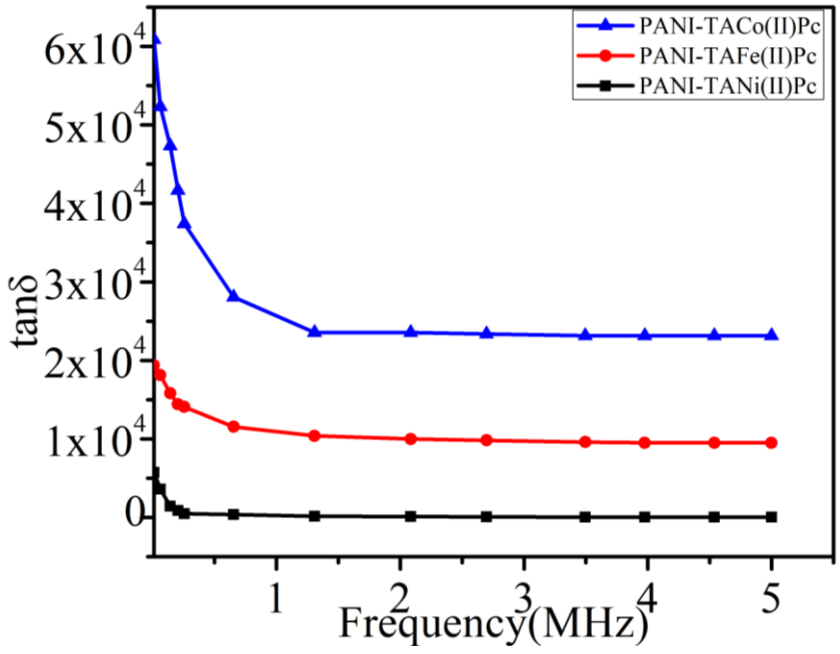

Figure 7. Variation of dielectric tangent loss of PANI-TAMPcs with frequency.

Also, the ability of dielectric loss of absorbing material sample is evaluated by the dielectric loss angle tangent tanδ = Ɛ”/Ɛ’. A better dielectric loss material must exhibit a large tanδ, which is independent of frequency. The variation of tanδ with frequency for the PANI-TAMPc nanocomposite at room temperature is shown in Figure 7. The tan δ decreases more rapidly at low frequencies and more slowly at higher frequencies. At higher frequencies, the electron exchange process is possible with very low energy consumption, since it is a region of very low resistivity compared to lower frequencies; thus, the loss is also less [27]. Among the three composites, PANI-TACo(II)Pc exhibits a higher dielectric loss tangent than PANI-TAFe(II)Pc and PANI-TANi(II)Pc.

3.7. AC conductivity studies.

Figure 8 demonstrates the frequency dependency of AC conductivity for the PANI-TAMPc nanocomposite at room temperature. At lower frequencies, the AC conductivity values do not change much at room temperature. It increases with higher frequency. This is in agreement with the theory of ac conduction in amorphous materials, which predicts that, for polaron transport or other hopping modes, electrical conductivity increases monotonically with the frequency of the applied field. Due to the activity of grain boundaries, the ac conductivity values are very low at lower frequencies due to reduced electron hopping. The conductive grains become increasingly active as frequency increases; this amplifies electron hopping between metal ions, thereby enhancing electrical conductivity [28]. At low frequencies, the AC conductivity shows only a slight frequency dependence, which may be associated with the uneven distribution of trapped charges within the polyaniline matrix. As the frequency increases, more trap sites become available for charge transport, thereby enhancing the conductive state through electron and hole hopping.

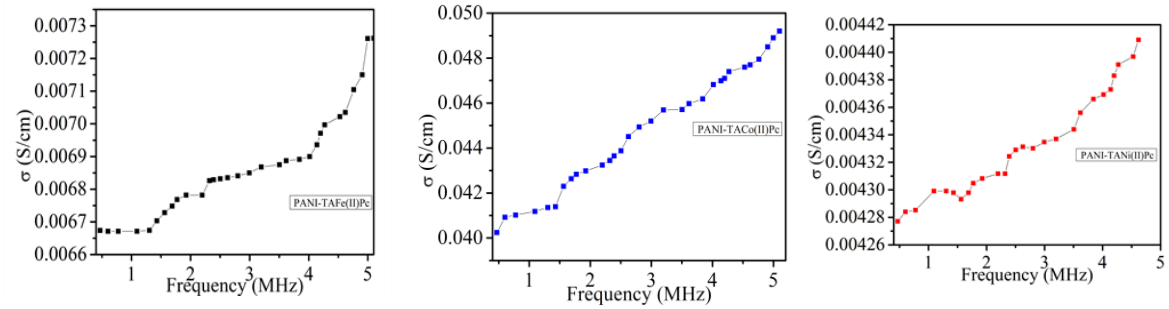

Figure 8. The variation of AC conductivity with frequency of PANI-TAMPcs.

The dielectric permittivity, ac conductivity, and dielectric loss can be related bythe following equation 2:

$$\sigma_{AC} = 2\pi\epsilon_0 \in' f tan\delta (2)$$

Where ϵ_0 is the permittivity of air and ϵ' is the dielectric permittivity of the sample, f is the frequency, and tanδ is the dielectric loss.

Among the three PANI-TAMPc composites, the PANI-TACo(II)Pc exhibits more conductivity than PANI-TAFe(II)Pc and PANI-TANi(II)Pc composites.

3.8. Electromagnetic interference shielding.

The major aspect that governs the electromagnetic interference shielding effectiveness (EMI SE) of a given composite is electrical conductivity, aspect ratio, dielectric properties, dispersion state of the filler in the matrix, and loading of the composite fillers [28,29].

Satisfactory electrical conductivity and dielectric behavior in nanocomposites can be achieved by incorporating highly conducting fillers. The determination of EMI SE of a given sample can be done by means of S parameters (S_{12}, S_{11}, S_{22}, S_{21}), which can be determined, and the EMI shielding mechanism can be schematically represented in Figure 9. The researchers have stated that the major mechanism in the sample material with an EMI SE value of ~10 dB is reflection and absorption, and that multiple reflections can be neglected in such cases [30,31]. The SE_R and SE_A can be calculated by S-parameters using the following equations:

$$SE_A = 10 \log_{10} \left(\frac{1-|S_{11}|^2}{|S_{12}|^2}\right) (3)$$

$$SE_R = 10 \log_{10} \left(\frac{1}{1-|S_{11}|^2}\right) (4)$$

Where SEA and SER are the EMI shielding effectiveness due to absorption and reflection, respectively, the EMI SE of a material can be estimated using a vector network analyzer.

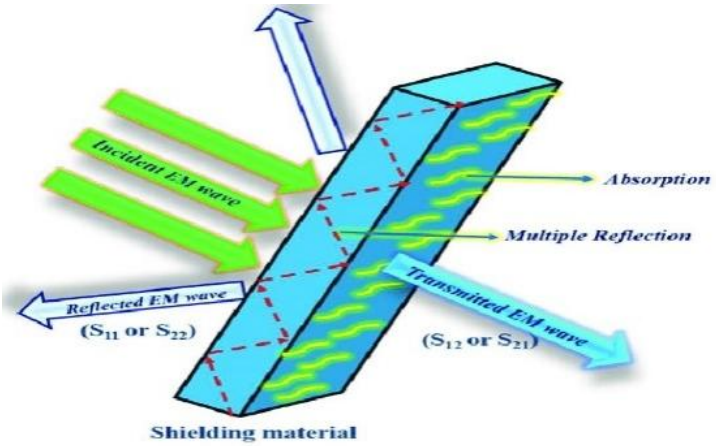

Figure 9. Schematic representation of the EMI shielding mechanism of the synthesized sample.

The scattering parameters S_{12} and S_{11} are referred to as the reverse transmission coefficient and forward reflection, respectively. The S parameters S_{12} and S_{11} are also used to calculate absorbed, reflected, and transmitted powers using the following relation.

$$R = |S_{11}|^2 + |S_{22}|^2 (5)$$

$$T = |S_{12}|^2 + |S_{21}|^2 (6)$$

$$A = 1 - R - T (7)$$

Where R, A, and T represent the reflected, absorbed, and transmitted powers, respectively.

Figure10aindicates the variation of absorption shielding effectiveness of PANI-TAMPcs and TACo(II)Pc with the frequency (8 GHz-12 GHz) in the X-band region. The PANI-TACo(II)Pc shows more absorption shielding effectiveness of 33dB than PANI-TAFe(II)Pc, PANI-TANi(II)Pc, and TACo(II)Pc. At the same time, Figure 10 b shows the variation of SE_R of the PANI-TAMPcs and TACo(II)Pc composite in the X-band. It can be observed that the PANI-TACo(II)Pc composites present lower SE_R values than PANI-TAFe(II)Pc, PANI-TANi(II)Pc, and TACo(II)Pc.

It can also be observed in Figure 10c that a large portion of the SET values is due to SE_A, and the SE_T varies in the same way as the SE_A. On the basis of the obtained results, it can be concluded that the attenuation of the electromagnetic wave is mainly due to electromagnetic absorption when probed into PANI-TACo(II)Pc nanocomposite [28,29]. This is essentially attributed to the richer interfacial polarization center at the TACo(II)Pc NPs-polyaniline polymer matrix interface, and to the rich charge carriers provided by TACo(II)Pc NPs [32,34].

Figures 10a,b, and c show a schematic representation of the EMI shielding of the PANI-TAMPc nanocomposite. Electromagnetic radiation was absorbed by the conducting PANI matrix and then by the 1D TAMPc-PANI nanocomposite, and these properties would result in distinctive electron transport or exciton emissions [35].

Furthermore, the specific surface area of the PANI increased upon the formation of a hierarchically nanostructured interphase of TACo(II) PcNP with cluster defects and multifunctional groups, which will regulate the Electromagnetic response, as well as dipole polarization and interfacial polarization of the material [36]. The interfacial attenuation between TACo(II)Pc NPs and PANI will result in electromagnetic wave attenuation within the multilayer structures. In order to absorb electromagnetic energy, electrons need to hop across the contact sites between the layers. Therefore, given its very high interfacial properties, among all other PANI-TAMPcs, the PANI-TACo(II)Pc can be an excellent candidate as an EMI shielding material for high-performance applications [37,39]. Table 1 shows the comparison of the EMI Shielding effectiveness of different nanocomposites with the synthesized PANI-TAMPc sample. This indicates that the synthesized PANI-TAMPc will be a highly effective material for attenuating electromagnetic signals.

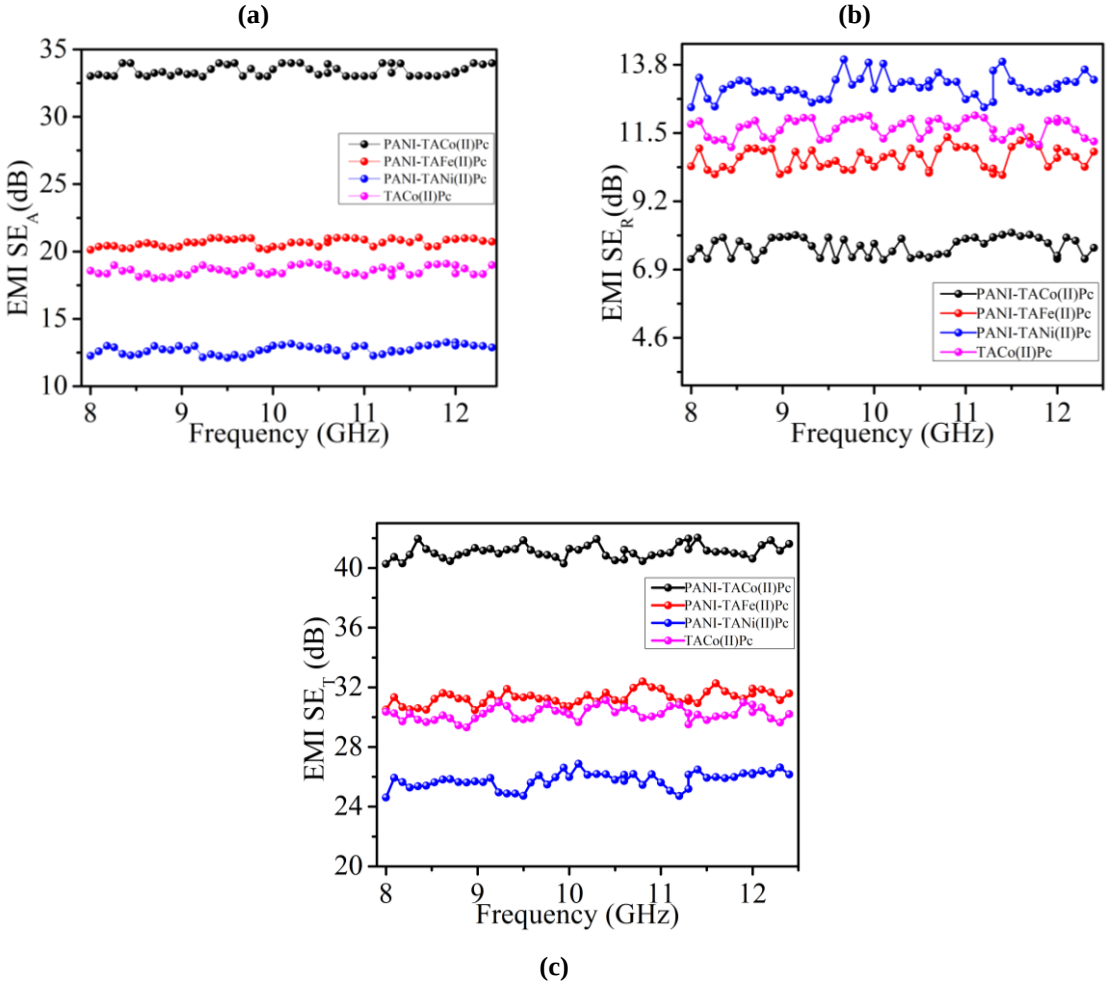

Figure 10. Variation of **(a)**SE_A values of TACo(II)Pc and PANI-TAMPc nanocomposite inX-Band; **(b)**SE_R values of TACo(II)Pc and PANI-TAM(II)Pcs nanocomposites in X-Band; **(c)**SE_T values of PANI-TAMPcs and TACo(II)Pc in X-Band.

Table 1. Comparative studies of the EMI shielding property of various reported materials under the optimal conditions.

Material	Frequency	SE_T (dB)	SE_A (dB)	SE_R (dB)	Thickness	Ref.
Polyaniline-flyash	12.4-18GHz	~30	~20	~10	2mm	[28]
Polyaniline- Y_2O_3	12.4-18GHz	~16	~13	~3	2.8mm	[29]

Material	Frequency	SE_T (dB)	SE_A (dB)	SE_R (dB)	Thickness	Ref.
Polyaniline-Antimony Oxide	12.4-18GHz	~21			2.8mm	[30]
PANI-MnO_2 nanorod	8.2-12.4GHz	~35	~24	~11	169±3μm	[31]
TACo(II)Pc	8.2-12.4GHz	~30	~18	~12	2mm	Present work
PANI-TACo(II)Pc	8.2-12.4GHz	~40	~33	~7	2mm	Present work
PANI-TAFe(II)Pc	8.2-12.4GHz	~31	~20	~11	2mm	Present work
PANI-TANi(II)Pc	8.2-12.4GHz	~25	~13	~12	2mm	Present work

3.9. Electrochemical characterization.

3.9.1. Charge transfer behavior of PANI-TACo(II)Pc electrode.

The study of the charge-transfer behavior of the PANI-TACo(II)Pc electrode was conducted using K4[Fe(CN)6] as a redox probe. The usual ferro/ferricyanide CV response can be exhibited by bare GCE, as shown in Fig 11(a), although it is well known that the PANI-TACo(II)Pc electrode shows a faster and more complete rate of electron transfer than bare GCE, as shown in Fig 11(b) [40]. This is due to the high surface area of the PANI nanocomposite GCE, which reduces the ΔE between cathodic and anodic potential peaks with a rise in current value; it facilitates good electron transfer between GCE and electrolyte

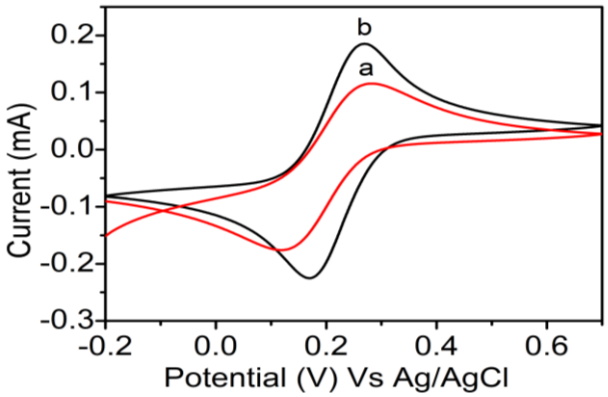

Figure 11. Cyclic voltammogram of **(a)** 0.5 M KCl solution consisting of 5mM of $K_3[Fe(CN)_6]/K_4[Fe(CN)_6]$ at GCE; **(b)** the PANI-TACo(II)Pc-GCE, scan rate: 50 mVs^{-1}.

3.9.2. Electrochemical characterization of different electrodes

The electrochemical detection of different electrodes can be studied through the CV technique both in the presence and absence of L-Cysteine in PBS of pH 7.0 at 0.2 to 0.8 V v/s Ag/AgCl at a scan rate of 50mVs^{-1}.

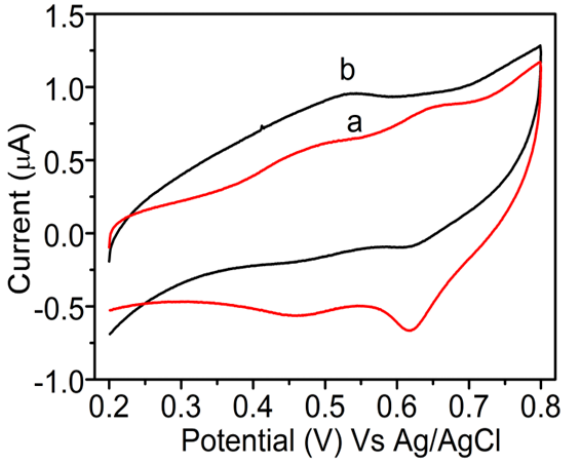

Figure 12. Cyclic voltamogram of **(a)** PANI-TACo(II)Pc/GCE in the absence of L-cysteine;**(b)** PANI-TACo(II)Pc/GCE in the presence of L-cysteine in a pH 7 buffer solution at the scan rate of 50mVs^{-1}.

It was observed that the PANI-TACo(II)Pc/GCE thin film increased the peak current by shifting the negative potential peak only slightly, in contrast to the modified electrode. Figure 12 indicates the Cyclic Voltamogram of (a) PANI-TACo(II)Pc/GCE and (b)PANI-TACo(II)Pc/GCE for a 0.5 µL concentration of L-Cysteine. The CV analysis of PANI-TACo(II)Pc/GCE alongside L-Cysteine was conducted in pH 7.0 PBS under an N_2 atmosphere, in which the modified PANI-TACo(II)Pc/GCE signal was situated at 0.52V. This indicates that PANI-TACo(II)Pc/GCE is well known to be very active in electrochemical and physicochemical properties [41].

3.9.3. Electro catalytic sensing of cysteine using PANI-TACo(II)Pc electrode.

A CV curve (Figure13) for the optimized PANI-TACo(II)Pc sensor towards L-cysteine of different concentrations was studied using cyclic voltammetry, and here, a buffer solution was used as an electrolyte; the CV scan was run at a fixed potential range of 0.2 V to 0.8 V at a pH 7.0 buffer solution [42,44]. The rise in the L-cysteine peak current concentration increases linearly. The modified electrode shows a good linearity calibration graph; the linear range, LOD, and sensitivity are 0.5-3.5 µM. The detection limit was 0.166 µM (Figures 2A and B), and the Sensitivity value is 0.1198 µA/µM, with a linear regression equation of Y = 0.1198X + 0.379 and a coefficient of correlation of 0.994. Thus, the nanocomposite material sensor can be applied for the detection of L-cysteine.

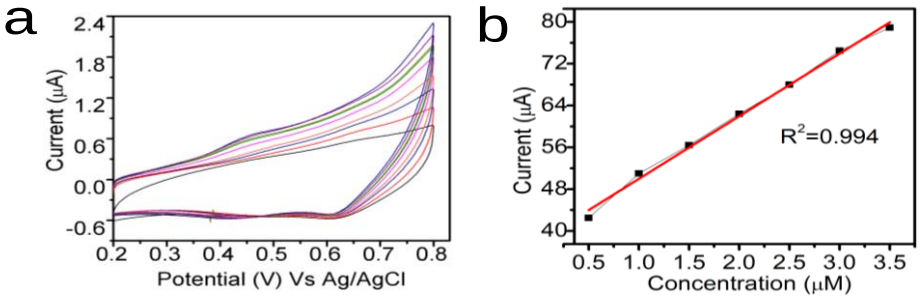

Figure 13. A CV of L-cysteine at PANI-TACo(II)Pc/GCE; the concentration ranges from (0.5–3.5 µM); b)Inset: Calibration plot for current Vs concentration.

To assess the stability of the modified electrode towards the catalytic oxidation of L-cysteine, we determined its stability in CV detection of L-cysteine by adding L-cysteine to the solution [45]. The detection of added L-cysteine was undertaken by the standard addition method. The results obtained for the analysis of L-cysteine by this method have been demonstrated many times in Table 2.

Table 2 . Determination of L-cystine in the phosphate buffer (pH 7.0).

Examination	Cysteine added (mg)	Cysteine found (mg)[a]	Recovery (%)	RSD (%)
1	1.27	1.25	98.42	3.1
2	1.31	1.27	96.94	2.4
3	1.35	1.29	95.55	2.0
4	1.39	1.41	101.4	1.9

3.9.4. Effect of scan rate.

CV voltamogram outline (Figure 14a) illustrates that the 3.5 µM L-cysteine in Phosphate buffer solution using the PANI-TACo(II)Pc sensor was tabulated for different scan rates (10-150 mVs^{-1}). It can be observed that the oxidative peak current also increases with increasing scan rate. The graph of oxidative peak current vs the square root of scan rate

demonstrates that the oxidation of L-cysteine on PANI-TACo(II)Pc/Glassy Carbon Electrode is a diffusion-controlled process [46]. The linear regression equation, I = 11.38υ + 0.288, and the coefficient of correlation, 0.9883, are shown in Figures 14a and 14b.

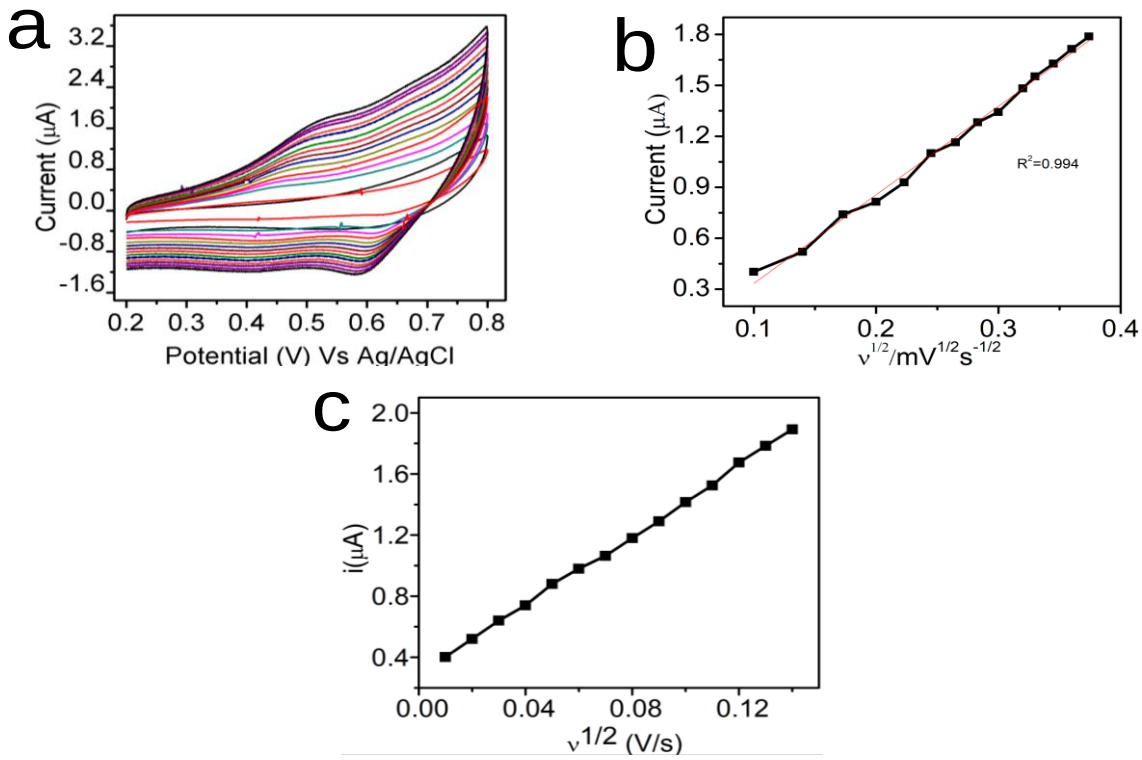

Figure 14. (a) CV of L-cysteine at PANI-TACo(II)Pc/GCE; scanning rate ranges from ($10mV^{-1}$ to 150 mVs^{-1}); **(b)** The plot of current Vs $υ^{1/2}/mV^{1/2}s^{-1/2}$; **(c)** Inset: Calibration graph of scan rate vs peak current.

3.9.5. Electrode stability and reproducibility.

The sensor was kept in phosphate buffer solution for 96 hours to assess its stability, and its response to L-cysteine was then tested. L-cysteine is oxidized at the same potential, and the current response was also the same as that obtained with freshly prepared sensors, indicating a stable response from the electrode [47,48]. This electrode shows high stability under dry conditions, even after being stored for 15 days. Also, the reproducibility of this sensor's response was evaluated by three consecutive analyses of L-cysteine using its voltammetric current. In these experiments, the RSD was 2.75% (n = 3, L-cysteine concentration = 10 µM), and the fabricated sensors showed satisfactory reproducibility (2.1%) [49].

3.9.6. Real sample analysis.

The PANI-TACo(II)Pc/GCE can be used to determine L-cysteine in the yogurt sample by cyclic voltammetry. Using standard additions, the recoveries of L-cysteine can be determined, and the results are tabulated in Table 3. To validate the practicality and reliability of this technique, the obtained recoveries were reasonable, ranging from 94.2% to 102.32%. Table 4 represents the comparison of the sensing of L-cysteineby using various electrodes with the PANI-TACo(II)Pc/GCE [50,51].

Table 3. Determination of L-cysteine in yogurt using PANI-TACo(II)Pc/GCE.

Sample	Added (µM)	Found (µM)	Recovery (%)
1	10.00	9.42±0.15	94.2
2	20.00	19.41±0.50	97.05
3	50.00	51.16±0.43	102.32
4	100.00	98.96±0.11	98.96

Table 4. Comparative study of PANI-TACo(II)Pc modified electrode with different modified electrodes in the detection of L-cysteine.

Electrode material	Method	Dynamic linear range(μM)	Detection limit(μM)	Sensitivity	Ref.
GO-Au NCs/GC	CV	0.05-20	0.02	-	[40]
CoPc-SPEs	CV	2.6-200	4	0.78 $\mu A \mu M^{-1} cm^{-2}$	[41]
RGO-pTACoPc	CV	0.05-2.0	0.018	10.19 $nA nM^{-1} cm^{-2}$	[42]
OMC/GCE	CV	18-2500	0.002	23.6 $\mu A \mu M^{-1} cm^{-2}$	[43]
PANI-TACo(II)Pc	CV	0.5-3.5	0.166	0.119$\mu A \mu M^{-1} cm^{-2}$	**This work**

4. Conclusions

A conducting polymer nanocomposite, PANI-TAMPc, was prepared by in situ polymerization of Aniline with TAMPc nanoparticles. The characterization of PANI-TAMPc nanocomposites was performed using XRD, SEM, FTIR, UV-Vis, and TGA. The frequency dependence of ac conductivity (σac) and dielectric permittivity has been investigated for PANI-TAMPc nanocomposites over the frequency range 40 Hz-5 MHz. The electrical conductivity of PANI-TAMPc nanocomposites is consistent with the electron-hopping model. It can be observed that PANI-TACo(II)Pc nanocomposite exhibits more electrical conductivity than the other PANI-TAMPcs. Further, the variation of EMI shielding effectiveness with frequency is studied. The EMI shielding effectiveness of the PANI-TACo(II)Pc nanocomposite was 40dB at X-band, which is higher than that of other PANI-TAMPcs, due to its higher dielectric permittivity and electrical conductivity, making it a good EMI shielding material. Additionally, the synthesized PANI-TACo(II)Pc/GCE can be used for the determination and sensing of L-cysteine, as well as in real samples, i.e., yogurt and a cysteine compound. All these results indicate that PANI-TACo(II)Pc can be an excellent EMI shielding material with high L-cysteine sensing performance.

Author Contributions

Conceptualization – M.P.; Methodology – N.T.N., J.S.; Software – M.P.; Validation – M.P.; Formal analysis – N.T.N.; Investigation – N.T.N., J.S.; Resources – N.T.N.; Data curation – N.T.N., M.P.; Writing – original draft preparation – N.T.N.; Writing – review & editing – J.S.; Visualization – N.T.N.; Supervision – J.S.; Project administration – J.S.; Funding acquisition – J.S., M.P. All authors have read and agreed to the published version of the manuscript.

Institutional Review Board Statement

Not applicable.

Informed Consent Statement

Not applicable.

Data Availability Statement

The data that support the findings of this study are available from the corresponding author upon reasonable request.

Funding

This research received no funding.

Acknowledgments

The authors wish to acknowledge the National College of Pharmacy for UV-Visible spectral data, the Karnataka University, Dharwad, and Mangalore University for imparting spectral data.

Conflicts of Interest

The authors have no conflicts of interest.

References

1. Riddle, A. Electromagnetic Interference (EMI). In Microwave and RF ProductApplications, 1st Edition; Golio, M., Ed.; CRC-Press: Boca Raton,Florida, USA, **2003**.
2. Zhang, L.; Bi, S.; Liu, M. Lightweight Electromagnetic Interference Shielding Materials and Their Mechanisms. In Electromagnetic Materials and Devices, Han, M.-G., Ed.; IntechOpen: London, **2018**;https://doi.org/10.5772/intechopen.82270.
3. Jabnoor, R.; B, M.; AmbikaPrasad, M.V.N.; Lagashetty, A.; Basavarajappa, V.; Kalyane, S. Synthesis, characterisation and AC conductivity study of PANI/α-Fe_2O_3 nanocomposites. *IOP Conf. Ser.: Mater. Sci. Eng.* **2022**, *1221*, 012001,https://doi.org/10.1088/1757-899X/1221/1/012001.
4. Ibanez, J.G.; Rincón, M.E.; Gutierrez-Granados, S.; Chahma, M.h.; Jaramillo-Quintero, O.A.; Frontana-Uribe, B.A. Conducting Polymers in the Fields of Energy, Environmental Remediation, and Chemical–Chiral Sensors. *Chem. Rev.* **2018**, *118*, 4731-4816, https://doi.org/10.1021/acs.chemrev.7b00482.
5. McKeown, N.B. Phthalocyanine-containing polymers. *J. Mater. Chem.* **2000**, *10*, 1979-1995, https://doi.org/10.1039/b000793p.
6. Pari, M.; Reddy, K.V. A facile Cobalt (II) tetra amino phthalocyanine ingrained poloy aniline (PANI) nano-fiber film layer based electrode material for amperometric determination of thiocyanate. *J. Inorg. Organomet. Polym. Mater.* **2020**, *30*, 3511-3520, https://doi.org/10.1007/s10904-020-01515-8.
7. Ambily, S.; Menon, C. Determination of the thermal activation energy and optical band gap of cobalt phthalocyanine thin films. *Mater. Lett.* **1998**, *34*, 124-127, https://doi.org/10.1016/S0167-577X(97)00151-1.
8. Zanguina, A.; Bayo-Bangoura, M.; Bayo, K.; Ouedraogo, G. IR and UV-visible spectra of iron (ii) phthalocyanine complexes with phosphine or phosphite. *Bull. Chem. Soc. Ethiop.* **2002**, *16*, 73-79, https://doi.org/10.4314/bcse.v16i1.20950.
9. Schramm, C.J.; Scaringe, R.P.; Stojakovic, D.R.; Hoffman, B.M.; Ibers, J.A.; Marks, T.J. Chemical, spectral, structural, and charge transport properties of the" molecular metals" produced by iodination of nickel phthalocyanine. *J. Am. Chem. Soc.* **1980**, *102*, 6702-6713, https://doi.org/10.1021/ja00542a008.
10. Pari, M.; Reddy, K.V. Amperometric determination of dopamine based on an interface platform comprising tetra-substituted Zn^{2+} phthalocyanine film layer with embedment of reduced graphene oxide. *Sens. Actuators, A, Phys.***2020**, *316*, 112377, https://doi.org/10.1016/j.sna.2020.112377.
11. Rajappa, S.; Shivarathri, P.G.; Kumari, M.L.A.; Swamygowda, D.K.; Devendrachari, M.C.; Kotresh, H.M.N. Mechanochemical route for tetra amino zinc phthalocyanine embedded PANI sensitized Fe_2O_3 heteroarchitecture for photodegradation of dyes under the influence of low power LED light source. *Surf. Interfaces* **2022**, *29*, 101720, https://doi.org/10.1016/j.surfin.2022.101720.
12. Walter, M.G.; Rudine, A.B.; Wamser, C.C. Porphyrins and phthalocyanines insolar photovoltaic cells.*J. Porphyr. Phthalocyanines* **2010**, *14*,759-792, https://doi.org/10.1142/S1088424610002689.
13. Flom, S.R.; Beadie, G.; Ponting, M. Nonlinear absorption and refraction in phthalocyanine-doped polymers. *Opt. Mater. Express* **2018**, *8*, 3955-3966, https://doi.org/10.1364/OME.8.003955.
14. Lever, A.; Hempstead, M.; Leznoff, C.; Liu, W.; Melnik, M.; Nevin, W.; Seymour, P. Recent studies in phthalocyanine chemistry. *Pure Appl. Chem.* **1986**, *58*, 1467-1476, https://doi.org/10.1351/pac198658111467.
15. Biswas, S.; Dagdelen, F.; Aydogdu, Y.; Dey, K. Structural, electrical and optical properties of metal complexes of NNS donor ligand. *Mater. Chem. Phys.* **2011**, *129*, 1121-1125, https://doi.org/10.1016/j.matchemphys.2011.05.071.

16. Mounesh; Sharan Kumar, T.; Praveen Kumar, N.; Venugopal Reddy, K. Poly (L-lactide)-carboxamide-CoPc with composite MWCNTs on glassy carbon electrode sensitive detection of hydrazine and L-cysteine. *Anal. Chem. Lett.* **2020**, *10*, 620-635, https://doi.org/10.1080/22297928.2020.1857835.
17. Achar, B.; Lokesh, K. Studies on tetra-amine phthalocyanines. *J. Organomet. Chem.* **2004**, *689*, 3357-3361, https://doi.org/10.1016/j.jorganchem.2004.07.045.
18. Boeva, Z.A.; Sergeyev, V.G. Polyaniline: Synthesis, properties, and application. *Polym. Sci. Ser. C* **2014**, *56*, 144-153, https://doi.org/10.1134/S1811238214010032.
19. Sudhakara, S.M.; Devendrachari, M.C.; Kotresh, H.M.N.; Khan, F. Silver nanoparticles decorated phthalocyanine doped polyaniline for the simultaneous electrochemical detection of hydroquinone and catechol. *J. Electroanal. Chem.* **2021**, *884*, 115071, https://doi.org/10.1016/j.jelechem.2021.115071.
20. Skripnikova, T.A.; Starikova, A.A.; Shumilova, G.I.; Ermolenko, Y.E.; Pendin, A.A.; Mourzina, Y.G. Towards stabilization of the potential response of Mn (III) tetraphenylporphyrin-based solid-state electrodes with selectivity for salicylate ions. *J. Solid State Electrochem.* **2017**, *21*, 2269-2279,https://doi.org/10.1007/s10008-017-3575-6.
21. Reddy, K.V.; Harish, M.; Khan, M.M.; Keshavayya, J. Synthesis, spectral, magnetic and thermal studies on symmetrically substituted metal(II)-1,3,8,10,15,17,22,24-octafluorophthalocyanines. *J. Fluor. Chem.***2007**, *128*, 1019-1025, https://doi.org/10.1016/j.jfluchem.2007.05.001.
22. Rani, N.S.; Sannappa, J.; Demappa, T. Effects of $CdCl_2$ concentration and gamma irradiation on the structural, thermal and electrical conductivity properties of HPMC polymer electrolyte films. *IOSR J. Appl. Phys.***2014**, *6*, 30-41, https://doi.org/10.9790/4861-06313041.
23. Madhu, B.; Gurusiddesh, M.; Kiran, T.; Shruthi, B.; Jayanna, H. Structural, dielectric, ac conductivity and electromagnetic shielding properties of polyaniline/$Ni_0.5Zn_{0.5}Fe_2O_4$ composites. *J. Mater. Sci.: Mater. Electron.* **2016**, *27*, 7760-7766, https://doi.org/10.1007/s10854-016-4764-2.
24. He, M.; Xu, P.; Zhang, Y.; Liu, K.; Yang, X. Phthalocyanine nanowires@ GO/carbon fiber composites with enhanced interfacial properties and electromagnetic interference shielding performance. *Chem. Eng. J.***2020**, *388*, 124255, https://doi.org/10.1016/j.cej.2020.124255.
25. Zhang, L.; Liu, M.; Roy, S.; Chu, E.K.; See, K.Y.; Hu, X. Phthalonitrile-based carbon foam with high specific mechanical strength and superior electromagnetic interference shielding performance. *ACS Appl. Mater. Interfaces***2016**, *8*, 7422-7430, https://doi.org/10.1021/acsami.5b12072.
26. Mphuthi, N.G.; Adekunle, A.S.; Fayemi, O.E.; Olasunkanmi, L.O.; Ebenso, E.E. Phthalocyanine doped metal oxide nanoparticles on multiwalled carbon nanotubes platform for the detection of dopamine. *Sci. Rep.* **2017**, *7*, 43181, https://doi.org/10.1038/srep43181.
27. Pauly, A.; Saad Ali, S.; Varenne, C.; Brunet, J.; Llobet, E.; Ndiaye, A.L. Phthalocyanines and porphyrins/polyaniline composites (PANI/CuPctBu and PANI/TPPH2) as sensing materials for ammonia detection. *Polymers* **2022**, *14*, 891, https://doi.org/10.3390/polym14050891.
28. Bora,P.J.; Vinoy, K.J.; Ramamurthy, P.C. Lightweight polyaniline-cobalt coated fly ashcenosphere composite film for electromagnetic Interference shielding. *Electron. Mater. Lett.* **2016**, *12*, 603-609, http://doi.org/10.1007/s13391-016-5447-0.
29. Faisal, M.; Khasim, S. Electrical Conductivity, Dielectric Behavior and EMI ShieldingEffectiveness of Polyaniline-Yttrium Oxide Composites. *Bull. Korean Chem. Soc.* **2013**, *34*, 99-106, https://doi.org/10.5012/bkcs.2013.34.1.99.
30. Faisal, M.; Khasim, S. Polyaniline–antimony oxide composites for effective broadband EMI shielding. *Iran. Polym. J.* **2013**, *22*, 473-480, https://doi.org/10.1007/s13726-013-0149-z.
31. Bora, P.J.; Vinoy, K.; Ramamurthy, P.C.; Madras, G. Electromagnetic interference shielding efficiency of MnO_2 nanorod doped polyaniline film. *Mater. Res. Express* **2017**, *4*, 025013, https://doi.org/10.1088/2053-1591/aa59e3.
32. Gao, H.; Wang, C.; Yang, Z.; Zhang, Y. 3D porous nickel metal foam/polyaniline heterostructure with excellent electromagnetic interference shielding capability and superior absorption based on pre-constructed macroscopic conductive framework. *Compos. Sci. Technol.* **2021**, *213*, 108896, https://doi.org/10.1016/j.compscitech.2021.108896.
33. Zahid, M.; Anum, R.; Siddique, S.; Shakir, H.F.; Rehan, Z. Polyaniline-based nanocomposites for electromagnetic interference shielding applications: A review. *J. Thermoplast. Compos. Mater.* **2023**, *36*, 1717-1761, https://doi.org/10.1177/08927057211022408.

34. Kausar, A. Nanocarbon nanocomposites of polyaniline and pyrrole for electromagnetic interference shielding: design and effectiveness. *Polym.-Plast. Technol. Mater.* **2022**, *61*, 1988-2000, https://doi.org/10.1080/25740881.2022.2086816.
35. Zhang, Y.; Pan, T.; Yang, Z. Flexible polyethylene terephthalate/polyaniline composite paper with bending durability and effective electromagnetic shielding performance. *Chem. Eng. J.* **2020**, *389*, 124433, https://doi.org/10.1016/j.cej.2020.124433.
36. Zubair, K.; Ashraf, A.; Gulzar, H.; Shakir, M.F.; Nawab, Y.; Rehan, Z.; Rashid, I.A. Study of mechanical, electrical and EMI shielding properties of polymer-based nanocomposites incorporating polyaniline coated graphene nanoparticles. *Nano Express* **2021**, *2*, 010038, https://doi.org/10.1088/2632-959X/abe843.
37. He, Z.; Xie, H.; Wu, H.; Chen, J.; Ma, S.; Duan, X.; Chen, A.; Kong, Z. Recent advances in MXene/polyaniline-based composites for electrochemical devices and electromagnetic interference shielding applications. *ACS Omega* **2021**, *6*, 22468-22477, https://doi.org/10.1021/acsomega.1c02996.
38. Nivedhitha, D.M.; Jeyanthi, S. Polyvinylidene fluoride—An advanced smart polymer for electromagnetic interference shielding applications—A novel review. *Polym. Adv. Technol.* **2023**, *34*, 1781-1806, https://doi.org/10.1002/pat.6015.
39. Omana, L.; Chandran, A.; John, R.E.; Wilson, R.; George, K.C.; Unnikrishnan, N.V.; Varghese, S.S.; George, G.; Simon, S.M.; Paul, I. Recent advances in polymer nanocomposites for electromagnetic interference shielding: a review. *ACS Omega* **2022**, *7*, 25921-25947, https://doi.org/10.1021/acsomega.2c02504.
40. Ge, S.; Yan, M.; Lu, J.; Zhang, M.; Yu, F.; Yu, J.; Song, X.; Yu, S. Electrochemical biosensor based on graphene oxide–Au nanoclusters composites for l-cysteine analysis. *Biosens. Bioelectron.* **2012**, *31*, 49-54, https://doi.org/10.1016/j.bios.2011.09.038.
41. Hernández-Ibáñeza, N.; Sanjuána, I.; Montiela, M.Á.; Fosterc, C.W.; Banksc, C.E.; Iniesta, J. L-Cysteine Determination in Embryo Cell Culture Media using Co (II)-phthalocyanine Nanoparticle Modified Disposable Screen-printed Electrodes. *J. Electroanal. Chem.***2016**, *780*, 303-310,https://doi.org/10.1016/j.jelechem.2016.09.028.
42. Mani, V.; Huang, S.-T.; Devasenathipathy, R.; Yang, T.C. Electropolymerization of cobalt tetraamino-phthalocyanine at reduced graphene oxide for electrochemical determination of cysteine and hydrazine. *RSC Adv.***2016**, *6*, 38463-38469, https://doi.org/10.1039/C6RA01851C.
43. Zhou, M.; Ding, J.; Guo, L.-p.; Shang, Q.-k. Electrochemical behavior of L-cysteine and its detection at ordered mesoporous carbon-modified glassy carbon electrode. *Anal. Chem.* **2007**, *79*, 5328-5335, https://doi.org/10.1021/ac0703707.
44. Prabhu, C.K.; Manjunatha, N.; Shambhulinga, A.; Imadadulla, M.; Shivaprasad, K.; Amshumali, M.; Lokesh, K.S. Synthesis and characterization of novel imine substituted phthalocyanine for sensing of L-cysteine. *J. Electroanal. Chem.* **2019**, *834*, 130-137, https://doi.org/10.1016/j.jelechem.2018.12.050.
45. Jilani, B.S.; Malathesh, P.; Mruthyunjayachari, C.; Reddy, K.V. Cobalt (II) tetra methyl-quinoline oxy bridged phthalocyanine carbon nano particles modified glassy carbon electrode for sensing nitrite: A voltammetric study. *Mater. Chem. Phys.* **2020**, *239*, 121920, https://doi.org/10.1016/j.matchemphys.2019.121920.
46. Ghomi, M.; Zare, E.N.; Varma, R.S. Properties of Conducting Polymers. In Conductive Polymers in Analytical Chemistry; ACS Symposium Series; American Chemical Society: **2022**; Volume 1405, pp. 39-65, https://doi.org/10.1021/bk-2022-1405.ch002.
47. Kazmi, S.J.; Nadeem, M.; Younis, A.; Loomba, S.; Shabbir, B.; Manzoor, S.; Hussain, S. PANI/CFO@ CNTs ternary composite system for EMI shielding applications. *J. Magn. Magn. Mater.***2022**, *563*, 170037, https://doi.org/10.1016/j.jmmm.2022.170037.
48. Khamcharoen, W.; Henry, C.S.; Siangproh, W. A novel L-cysteine sensor using in-situ electropolymerization of L-cysteine: Potential to simple and selective detection. *Talanta* **2022**, *237*, 122983,https://doi.org/10.1016/j.talanta.2021.122983.
49. Musarraf Hussain, M.; Asiri, A.M.; Uddin, J.; Marwani, H.M.; Rahman, M.M. Development of a L-cysteine sensor based on thallium oxide coupled multi-walled carbon nanotube nanocomposites with electrochemical approach. *Chem. Asian J.* **2022**, *17*, e202101117, https://doi.org/10.1002/asia.202101117.
50. Hou, H.; Tang, S.; Wang, W.; Liu, M.; Liang, A.; Sun, L.; Luo, A. Electrochemical Enantioanalysis of D-and L-Cysteine with a Dual-Template Molecularly Imprinted Sensor. *J. Electrochem. Soc* **2022**, *169*, 037506, https://doi.org/10.1149/1945-7111/ac58c0.

51. Jalali, A.; Zhang, R.; Rahmati, R.; Nofar, M.; Sain, M.; Park, C.B. Recent progress and perspective in additive manufacturing of EMI shielding functional polymer nanocomposites. *Nano Res.***2023**, *16*, 1-17, https://doi.org/10.1007/s12274-022-5053-4.

Publisher's Note & Disclaimer